

# Orbit Determination of KOMPSAT-1 and Cryosat-2 Satellites Using Optical Wide-field Patrol Network (OWL-Net) Data with Batch Least Squares Filter

Eunji Lee<sup>1</sup>, Sang-Young Park<sup>1†</sup>, Bumjoon Shin<sup>1</sup>, Sungki Cho<sup>2</sup>, Eun-Jung Choi<sup>2</sup>, Junghyun Jo<sup>2</sup>, Jang-Hyun Park<sup>2</sup>

<sup>1</sup>Department of Astronomy, Yonsei University, Seoul 03722, Korea

<sup>2</sup>Korea Astronomy and Space Science Institute, Daejeon 34055, Korea

The optical wide-field patrol network (OWL-Net) is a Korean optical surveillance system that tracks and monitors domestic satellites. In this study, a batch least squares algorithm was developed for optical measurements and verified by Monte Carlo simulation and covariance analysis. Potential error sources of OWL-Net, such as noise, bias, and clock errors, were analyzed. There is a linear relation between the estimation accuracy and the noise level, and the accuracy significantly depends on the declination bias. In addition, the time-tagging error significantly degrades the observation accuracy, while the time-synchronization offset corresponds to the orbital motion. The Cartesian state vector and measurement bias were determined using the OWL-Net tracking data of the KOMPSAT-1 and Cryosat-2 satellites. The comparison with known orbital information based on two-line elements (TLE) and the consolidated prediction format (CPF) shows that the orbit determination accuracy is similar to that of TLE. Furthermore, the precision and accuracy of OWL-Net observation data were determined to be tens of arcsec and sub-degree level, respectively.

**Keywords:** orbit determination, optical surveillance, OWL-Net, batch least squares filter, KOMPSAT-1, Cryosat-2

## 1. INTRODUCTION

Optical observation has been used to detect space objects and a considerable number of optical observation systems are available such as the ground-based electro-optical deep space surveillance (GEODSS; Henize et al. 1993), Lincoln near-Earth asteroid program (LINEAR; Stokes et al. 2000), and international scientific optical network (ISON; Molotov et al. 2008). The optical observation system is appropriate for the surveillance of space objects because it is not limited by the range to the object, unlike active tracking systems such as radar and laser. For this reason, a lot of research on orbit determination (OD) using optical measurements has been conducted. Sabol et al. (2007) developed a simplified covariance model to predict the orbital error uncertainty

and demonstrated that high-accuracy orbit updates from angle-only data are available only if the eccentricity has a low uncertainty. Vallado & Agapov (2010) introduced OD results of geosynchronous (GEO) satellites using high-quality optical data from ISON; an uncertainty of ~5 km was obtained using the least squares method. Tombasco (2011) addressed GEO orbit estimation using ground-based and space-based angle-only measurements and enhanced the accuracy based on GEO elements.

The optical wide-field patrol network (OWL-Net) is an optical surveillance system of space objects developed at the Korea Astronomy and Space Science Institute (KASI). The main goals of the system are the tracking and monitoring of domestic satellites to protect space assets. There are five observatories around the world, in Korea, Mongolia, Morocco,

© This is an Open Access article distributed under the terms of the Creative Commons Attribution Non-Commercial License (<https://creativecommons.org/licenses/by-nc/3.0/>) which permits unrestricted non-commercial use, distribution, and reproduction in any medium, provided the original work is properly cited.

Received 25 AUG 2016 Revised 27 FEB 2017 Accepted 28 FEB 2017

†Corresponding Author

Tel: +82-2-2123-5687, E-mail: spark624@yonsei.ac.kr

ORCID: <https://orcid.org/0000-0002-1962-4038>

Israel, and the USA. The OWL-Net provides topocentric right ascension and declination measurement data converted from the image pixel coordinates (Park et al. 2013).

The orbital states of low earth orbit (LEO) satellites were evaluated in previous studies based on OWL-Net data. Jo et al. (2015) utilized commercial OD software to achieve preliminary OD results and showed that the requirements of OD can be achieved. In another study, Park et al. (2015) utilized the same software and analyzed the OD accuracy according to the number of estimation points.

In this study, OD software for the optical surveillance of space objects was developed and the orbital states of two LEO satellites, KOMPSAT-1 and Cryosat-2, were determined using the software and OWL-Net data. In addition, the precision and accuracy of OWL-Net data were analyzed based on the simulation of potential error sources of OWL-Net measurements such as noise, bias, and clock errors. The software is available to operate independent optical surveillance systems of space objects.

The batch least squares algorithm is introduced and verified in Section 2. The error sources of the OWL-Net are analyzed in Section 3. The estimation results using actual data are addressed and compared with known orbital information in Section 4 and Section 5 summarizes this paper.

## 2. BATCH LEAST SQUARES FILTER

The batch least squares algorithm is a post-processing estimation algorithm known as differential correction. It processes all data in a lump to determine the epoch states. Although this procedure is not appropriate for real-time systems, it is generally used because of some advantages. The batch estimation is simple and more accurate and robust compared with sequential estimation algorithms, such as the Kalman filter (Crassidis & Junkins 2011).

This section mathematically describes the algorithm including definitions of cost function, covariance matrix, and convergence criteria.

### 2.1 Methodology

The batch least squares algorithm estimates epoch states using a system model (F):

$$Y = F(X) + \epsilon \tag{1}$$

In case of OD, Y is the measurement data set,  $\epsilon$  is the measurement noise vector, and X is a solve-for-vector, which is required such as the position and velocity vector (Schutz et

al. 2004). The system model can be separated into dynamic and measurement models.

The estimation can be referred to as an optimization, which minimizes the cost function (Q), weighted sum of the squares of the measurement residual, and the difference from *a priori* states:

$$Q(\bar{X}) = [Y - F(X)]^T W [Y - F(X)] + [X - X_0]^T [P_{\Delta X_0}]^{-1} [X - X_0] \tag{2}$$

where  $P_{\Delta X_0}$  and  $X_0$  are the *a priori* covariance matrix and state vector, respectively, and W is the weight matrix. The *a priori* covariance matrix and weight matrix reflect the *a priori* uncertainty and measurement white noise, respectively:

$$P_{\Delta X} = \text{diag}([\sigma_1^{-2} \dots \sigma_n^{-2}])^{-1} \tag{3}$$

where  $\sigma_j$  is the standard deviation of the  $j^{\text{th}}$  element of the solve-for-vector, n is the dimension of the solve-for vector, and m is the number of measurement data.

If the *a priori* states are close enough to the true states, the system model and cost function can be linearized using the Taylor expansion. Hence, a normal equation is derived to evaluate the variate of the  $i^{\text{th}}$  iteration ( $\Delta X_i$ ) and the solve-for-vector is then updated (Long et al. 1989):

$$\Delta \hat{X}_i = (H^T W H + P_{\Delta X_0}^{-1})^{-1} (H^T W \Delta Y_i + P_{\Delta X_0}^{-1} (\Delta \hat{X}_{i-1} - X_0)) \tag{4}$$

$$\hat{X}_i = \hat{X}_{i-1} + \Delta \hat{X}_i$$

where H is the Jacobian matrix, a partial derivative of the system model. It can be divided into state transition matrix ( $\Phi$ ) and sensitivity matrix (A) using the chain rule.

$$H = A \Phi \tag{5}$$

When the solve-for-vectors are the Cartesian position and velocity vector ( $X = [r_1 \ r_2 \ r_3 \ v_1 \ v_2 \ v_3]^T$ ), and the measurement data consist of topocentric right ascension ( $\alpha$ ) and declination ( $\delta$ ), the sensitivity matrix is simply formulated:

$$A = \begin{bmatrix} \frac{\partial \alpha}{\partial X} & \frac{\partial \delta}{\partial X} \end{bmatrix}^T = \begin{bmatrix} -\frac{\rho_2}{\rho_1^2 + \rho_2^2} & \frac{\rho_1}{\rho_1^2 + \rho_2^2} & 0 & 0 & 0 & 0 \\ -\frac{\rho_1 \rho_3}{\rho^2 \sqrt{\rho_1^2 + \rho_2^2}} & \frac{\rho_2 \rho_3}{\rho^2 \sqrt{\rho_1^2 + \rho_2^2}} & \frac{\sqrt{\rho_1^2 + \rho_2^2}}{\rho^2} & 0 & 0 & 0 \end{bmatrix} \tag{6}$$

where  $\rho$  is the relative position vector of the object with respect to the observatory ( $R_{\text{obs}} = [r_{\text{obs},1} \ r_{\text{obs},2} \ r_{\text{obs},3}]$ ), i.e.,  $\rho = [\rho_1, \rho_2, \rho_3] = [r_1 - r_{\text{obs},1}, r_2 - r_{\text{obs},2}, r_3 - r_{\text{obs},3}]$ . If the measurement bias ( $\beta$ ) is also estimated, following terms are added to the Jacobian matrix:

$$\frac{\partial \mathbf{F}}{\partial \boldsymbol{\beta}} = k \times \begin{bmatrix} 1 & 0 \\ 0 & 1 \end{bmatrix} \quad (7)$$

where  $k$  is the scaling parameter, which is set to one by default.

The whole process, which includes the prediction and update, is iterated until convergence is achieved. The convergence criterion is the cost reduction ratio ( $\gamma$ ):

$$\gamma = \frac{Q_i - Q_{i-1}}{Q_i} \quad (8)$$

The estimation sequence is finished if the ratio becomes less than a small tolerance ( $\varepsilon$ ) set as  $10^{-3}$  by default, and it also terminated if the ratio is negative, which means increasing cost and maximum number of iterations are reached.

The covariance matrix ( $\mathbf{P}$ ), which contains the statistical information of the estimation, is evaluated after convergence. The covariance matrix is evaluated as follows:

$$\mathbf{P}_{\Delta \mathbf{x}} = (\mathbf{H}^T \mathbf{W} \mathbf{H} + \mathbf{P}_{\Delta \mathbf{x}_0}^{-1})^{-1} \quad (9)$$

In this study, the general mission analysis tool (GMAT) is used as the dynamic model (Hughes et al. 2014) and the state transition matrix is numerically evaluated.

## 2.2 Algorithm Verification

The covariance matrix estimated from the estimation algorithm has a statistical meaning and addresses the precision of the estimation. To confirm the validity of the estimated covariance matrix, Monte Carlo simulations were conducted and the results were compared. If the estimated

covariance is equal to the results, the estimation is valid.

Monte Carlo simulation was conducted for two different cases: states estimation with unbiased measurement data (Case 1) and states and bias estimation with biased measurement data (Case 2). Each case is simulated 1,000 times using the LEO. Table 1 lists the detailed configuration of the simulation. Instead of GMAT, two-body dynamics were assumed for simplification purposes based on the statistical independence of the system model. The pseudo-measurement properties of the OWL-Net measurement are as follows: the pass length is an observable period; exposure time is the time when taking a picture; exposure period is the timespan between two pictures; the data frequency is the number of extracted data points per second.

The precision of the estimation can be evaluated by the integration of a multivariable probability function. Especially in the case of multivariable space, several methods can be used to interpret the uncertainty of the variables such as the hyper-rectangle and hyper-ellipsoid methods (Long et al. 1989). The probability that the three-dimensional position vector is within the  $3\sigma$  range, for instance, is  $\sim 97\%$  and  $\sim 99\%$  based on the hyper-ellipsoid and hyper-rectangle methods, respectively. In this study, the hyper-ellipsoid method was used because the hyper-rectangle probability is a simple extension of the single Gaussian probability function.

In both cases, the algorithm was verified based on the statistical significance (97%) of the results of the covariance ellipsoid. Fig. 1 shows the comparison between the results of the Monte Carlo simulation and the estimated covariance ellipsoid for both cases. Note that they are used only for algorithm verification and not for performance validation.

**Table 1.** Simulation environment for the verification of the batch least squares algorithm

Property		Value	
		Case 1	Case 2
Orbit	Epoch Time (UTC)	02 May 2010 00:01:04.000	
	Semi-Major Axis (km)	7,194.995	
	Eccentricity	0.001	
	Inclination ( $^\circ$ )	97.507	
	Right Ascension of Ascending Node ( $^\circ$ )	117.725	
	Argument of Perigee ( $^\circ$ )	208.630	
	True Anomaly ( $^\circ$ )	285.493	
Dynamic Model		2-body (Matlab mex)	
Estimation	Convergence Criteria	$10^{-3}$	
<i>A priori</i> Uncertainty	Position (km)	1	
	Velocity (km/s)	0.001	
Measurement	Pass Length (sec)	300	
	Exposure Time (sec)	4	
	Exposure Period (sec)	20	
	Data Frequency (sec)	10	
	Noise (arc-sec)	1	
	Bias ( $^\circ$ )	None	0.1

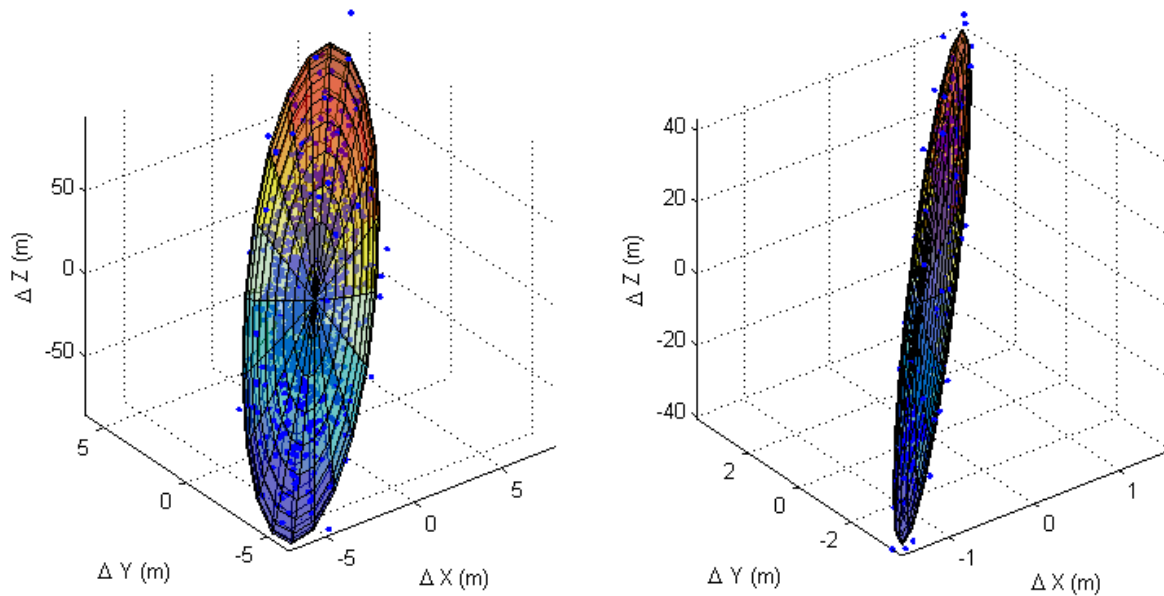


**Fig. 1.** Comparison between the results of the Monte Carlo simulation and covariance ellipsoid under different conditions; measurement bias exists and is estimated (left); it does not exist and is not estimated (right); 97 % of the results plot inside the covariance ellipsoid in both cases, which means that the algorithm has statistical significance.

**Table 2.** Simulation environments for all types of error analyses

Property		Value
Orbit	Epoch Time (UTC)	02 Feb 2016 03:00:59.600
	Semi-Major Axis (km)	7,094.1112
	Eccentricity	2.7417e-4
	Inclination (°)	97.6172
	Right Ascension of Ascending Node (°)	117.7144
	Argument of Perigee (°)	240.6593
	True Anomaly (°)	269.1909
Dynamic Model		EGM96 40 × 40 3 <sup>rd</sup> body gravity (Sun, Moon and 9 planets, DE405) Solar Radiation Pressure Air drag (Jacchia-Roberts)
Estimation	Convergence Criteria	10 <sup>-3</sup>
<i>A priori</i> Uncertainty	Position (km)	10
	Velocity (km/s)	0.01
Measurement	Pass Length (sec)	300
	Exposure Time (sec)	4
	Exposure Period (sec)	20
	Data Frequency (sec)	10

### 3. ERROR ANALYSIS

As opposed to the simulated observation, which only has Gaussian white noise, the real observation has more error sources such as bias and clock errors. In this section, the effects of noise, bias, and clock errors are determined using simulations of pseudo-measurement data. The analyzed relationship of each error source with the OD result can be used to interpret and predict the actual OD result. Table 2 lists common environments of all types of error analyses.

#### 3.1 Noise

Noise is a random error generated by thermal radiation. It is equal to the precision of the observation and cannot be exactly estimated and corrected. To check the effect of noise on the accuracy of the estimation, the OD simulations were conducted 100 times using pseudo-measurements and varying noise levels from 1 to 150 arcsec without bias. Note that the range of noise level is set as a known property of the OWL-Net measurement.

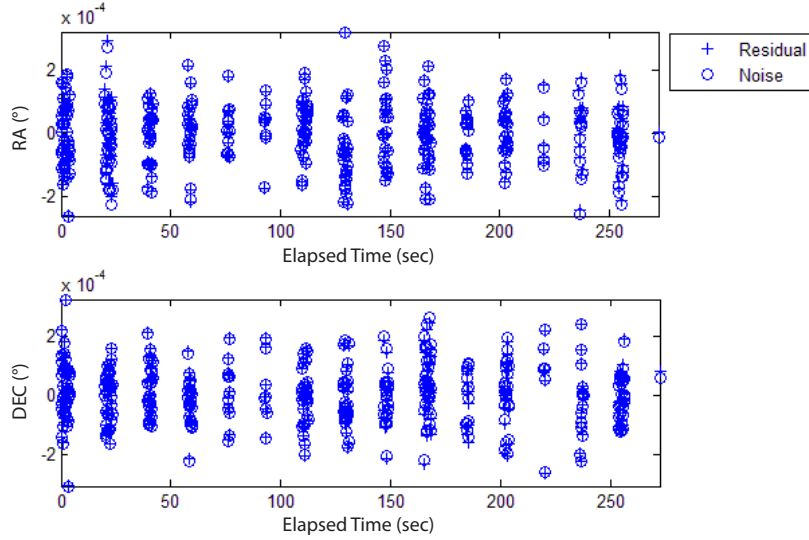


Fig. 2. Comparison between the noise and residual, which are distributed in the same pattern.

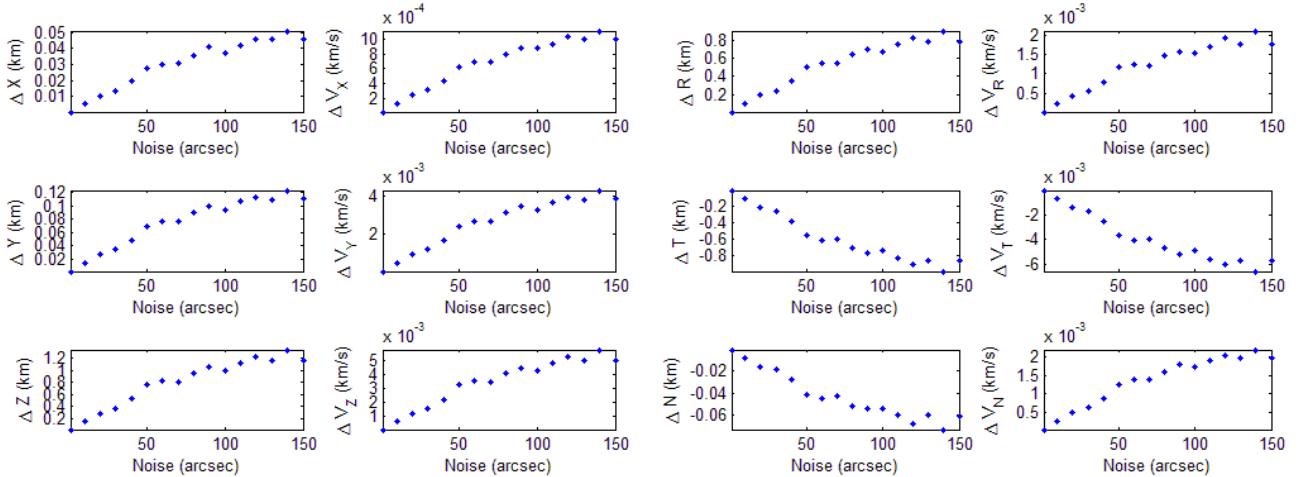


Fig. 3. Noise effect on the accuracy of the orbit estimation in ECI (left) and RTN (right) coordinates. The RMS error of each state linearly depends on the noise level and most position errors are concentrated in the z-axis and radial component.

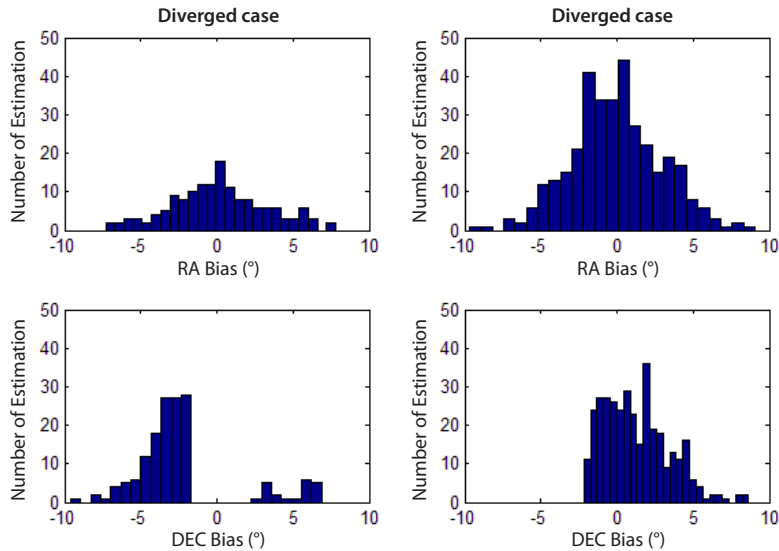
As a result, the residual exhibits the same distribution as the noise but without any trend (Fig. 2), which means that the resultant residual distribution can be conversely used to analyze the observation quality. In addition, the developed batch least squares filter reduces the *a priori* state error irrespective of the measurement noise.

Fig. 3 shows the root-mean-square (RMS) error of each state in earth centered inertial (ECI) and radial-tangential-normal (RTN) coordinates. It is directly proportional to the noise level, that is, the observation precision, and much smaller than the *a priori* error. The magnitude of the position error depends on the axis, especially that of the z-axis and radial error are larger than that of other axes. This might be due to the characteristics of the optical observation, which cannot include the line of sight direction information.

### 3.2 Bias

Bias can be caused by various factors such as coordinate transformation, catalog matching errors, and clock errors (Son et al. 2015). Although it might not be a constant due to the nonlinearity of the system, it is considered as a constant for a short arc for simplicity in this paper. To examine how the bias affects the OD, the OD simulations were conducted 500 times using pseudo-measurements. The pseudo-measurements are generated with a random bias of  $3^\circ$  ( $1\sigma$ ), which is not estimated, and a noise level of 40 arcsec. Note that the magnitude of the bias is set large enough to include many bias causes.

Approximately 70 % of the estimations converged; however, only 35 % of them converged with a proper answer and 30 % of



**Fig. 4.** Bias distribution comparison between the diverged and converged case. The RA bias shows no tendency; however, the DEC bias does. The estimation converges only if the DEC bias is smaller than  $\sim 2^\circ$ .

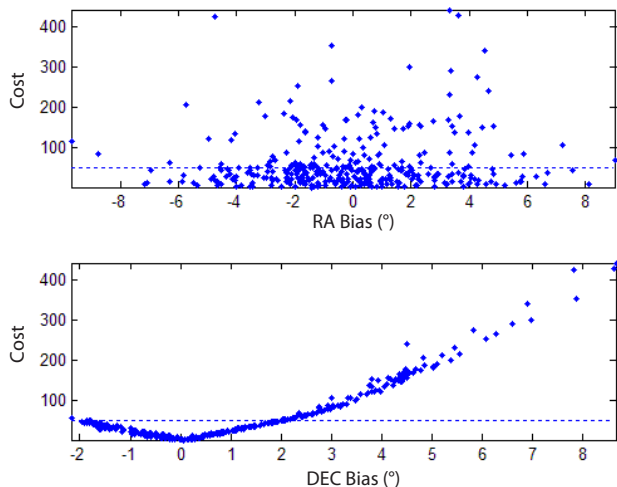


**Fig. 5.** Cost distribution of convergence cases with respect to RA and DEC bias. The RA bias is randomly distributed independent of the cost. The DEC bias is, in contrast, notably separated by the criterion.

the estimations even terminated in divergence. The results do not depend on the right ascension (RA) bias but they strongly depend on the declination (DEC) bias (Fig. 4). The estimation converges only if the DEC bias is larger than approximately  $-2^\circ$ , whereas there is no dependence on the RA bias. The estimation accuracy of the normal cases is on the order of kilometers and that of wrong cases is on the order of several hundreds of kilometers. A separation criterion between normal and wrong cases is the cost (Eq. (2)) of 50, where the cost of unity represents that the *a priori* error is removed and the residual is normalized. Fig. 5 shows that the RA bias is randomly distributed, regardless of the criterion, while the DEC bias is notably separated due to the criterion.

This result probably depends on the orbit. Because the simulated orbit is almost polar (inclination of  $97^\circ$ ), the declination changes more than the right ascension and the DEC bias is more influential than the RA bias. The relationship between the orbital characteristics and the effect of bias will be analyzed in the future.

### 3.3 Clock Error

The OWL observatory synchronizes time using a network time protocol (NTP) server, which has a precision on the order of 0.001 sec (Son et al. 2015). The data reduction algorithm includes a step to combine the extracted data points and time log (Park et al. 2013) based on which two types of clock errors are simulated. The first error is the time-synchronization offset (Case 1), where the whole time log is shifted. The other error is the time-tagging error (Case 2), where parts of the time logs are shifted. In case of the time-tagging error, the portions of the shifted observation are 25 % (Case 2-1), 50 % (Case 2-2), and 75 % (Case 2-3). All cases are simulated 100 times with a noise level of 15 arcsec corresponding to the OWL-Net without bias.

Fig. 6 describes the effects of all types of clock errors onto the position and velocity. In case of the time-synchronization offset, the position error ranges from 1.5 to 7.6 km because the offset increases from 0.2 to 1 sec. The result corresponds to the orbital motion of LEO ( $\sim 7$  km/s). In contrast to the overall time offset, the time-tagging error is an error source that leads to irregular observation data. In Case 2-1, the cost is minimized when the estimated state corresponds to the normal measurement

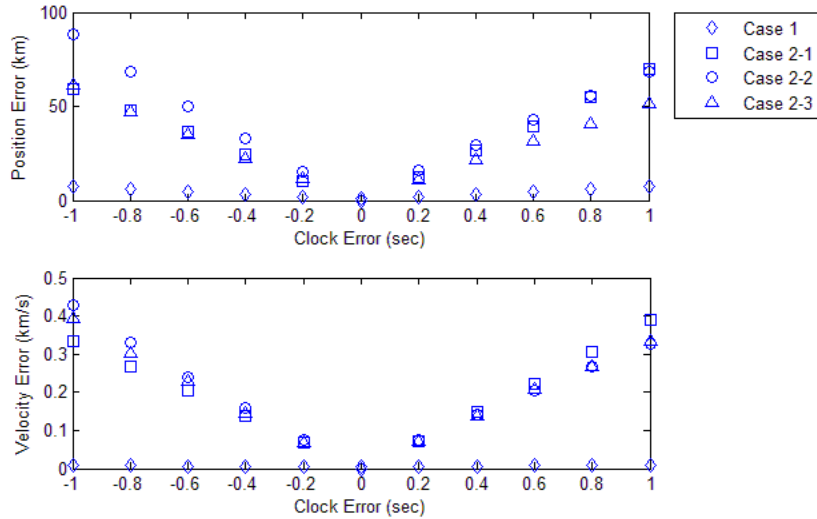


**Fig. 6.** Clock error effect on the estimation accuracy. Depending on the time-synchronization offset (Case 1), the position error ranges from 1.5 to 7.6 km, which corresponds to the orbital motion of LEO of  $\sim 7$  km/s. In Case 2, the state error increased up to  $\sim 90$  km. In contrast to the time-synchronization offset, the time-tagging error leads to irregular observation data and the accuracy declines.

because only 25 % of the measurement data have clock errors. On the other hand, 75 % of the measurement data have clock errors in Case 2-3 and the estimation thus corresponds to the error measurement. The estimation error is largest because the normal and abnormal measurements occupy the same portion in Case 2-2. In conclusion, the biggest state error is  $\sim 90$  km in Case 2-2; Cases 2-1 and 2-3 have a similar level of state error.

## 4. OWL-NET APPLICATION

The OWL-Net observation data (topocentric right ascension,  $\alpha$ , and declination,  $\delta$ ) of two LEO satellites, KOMPSAT-1 and Cryosat-2, are available. KOMPSAT-1 is a Korean Earth observation satellite at an altitude of 685 km, which was launched in 1999 and completed its mission in 2008 (Kim et al. 2015). Cryosat-2, is another Earth observation satellite mission managed by the European Space Agency (ESA). It was launched in 2010 and measures the thickness of sea ice using radar altimetry at an altitude of 725 km (Kurtz et al. 2014). The data were applied to the estimation algorithm, which was verified to provide reliable estimation results. Furthermore, the characteristics of OWL-Net observation data were determined based on the error analysis explained in Section 3.

### 4.1 Data Overview

The OWL-Net observation data were provided in form of report files, which include the name of the target satellite, location of the observatory, exposure time, charged-coupled

device (CCD) temperature, and time-tagged data points. Each file reflects a tracking pass of the satellite and consists of pictures from which the data points were extracted. Fig. 7 shows the data points extracted from a report file of KOMPSAT-1 and Cryosat-2. The arc of 4 min measured on November 5, 2014, and the arc of 5 min measured on May 25, 2015, were used for KOMPSAT-1 and Cryosat-2, respectively. Note that the properties of the arc, such as length, extraction period, and number of data points, are different in the two cases.

### 4.2 Orbit Determination

The orbit of each satellite was determined using OWL-Net observations and the developed algorithm (Section 2). The OD is conducted with and without bias estimation. The results of the Gauss method, which is one of the initial OD techniques, were used as *a priori* states. Other configuration details are listed in Table 3.

In case of KOMPSAT-1, the residual uniformly decreased from about  $0.1^\circ$  to 14 arcsec throughout the whole observation for both RA and DEC (Fig. 8). The estimated biases are  $0.2738^\circ$  and  $-0.0148^\circ$  for RA and DEC, respectively.

The residuals of Cryosat-2 also reduced from several degrees to  $\sim 0.1^\circ$  after OD processing. The pattern, however, is quite distinct from that of KOMPSAT-1; the residual is not uniform but exceptionally large in the beginning and end of the observation (Fig. 9). For this reason, only the middle part of Cryosat-2 data was used for OD, that is, data editing. To exclude abnormal measurement data from the OD process, data points extracted from specific pictures were removed, while the editing

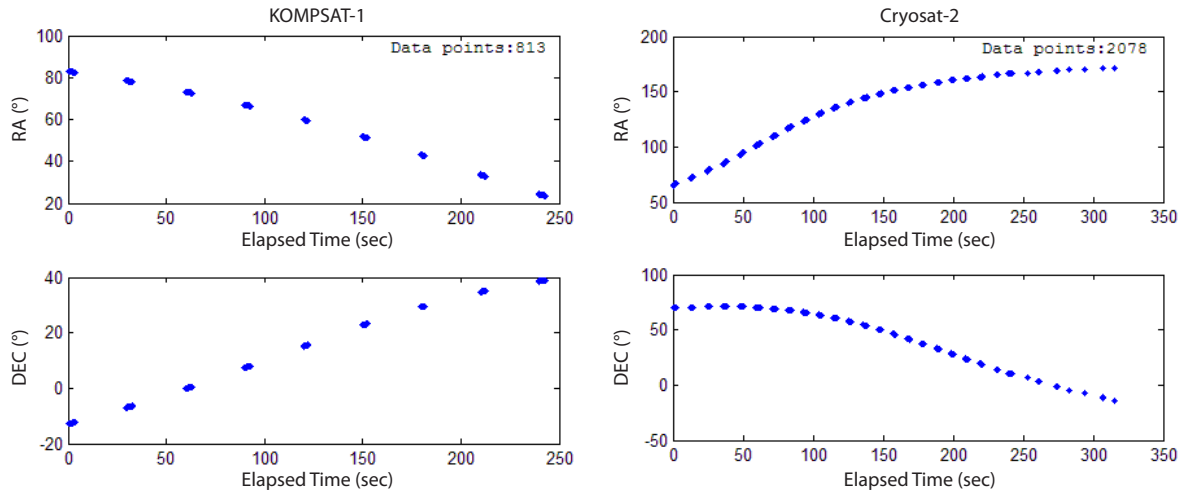


**Fig. 7.** Data points extracted from the report file of KOMPSAT-1 (left) and Cryosat-2 (right). Properties such as arc length, extraction period, and number of data points differ from arc to arc.

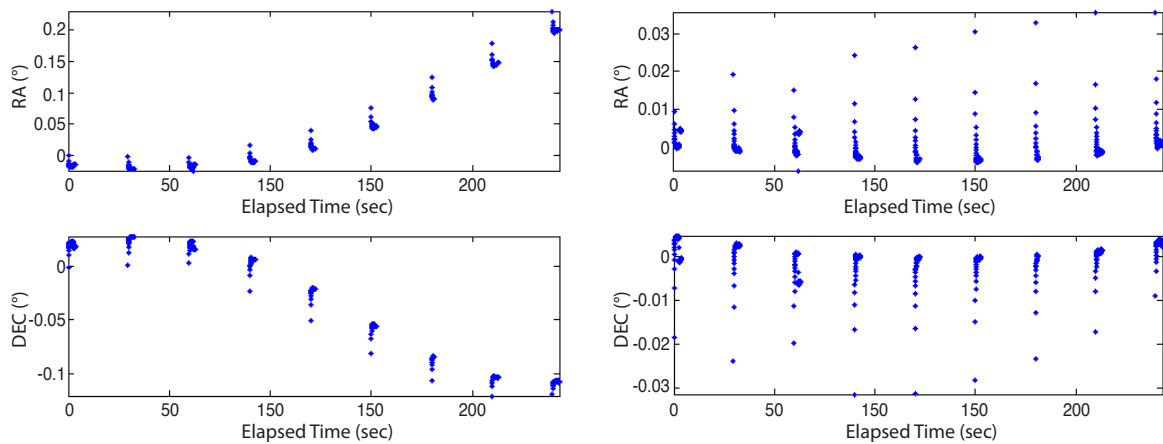


**Fig. 8.** *A priori* residual (left) and final residual after convergence (right) in the case of KOMPSAT-1. The residual decreased from  $\sim 0.1^\circ$  to 14 arc seconds and is uniform throughout the whole observation for both RA and DEC.

**Table 3.** Configuration of the OD for KOMPSAT-1 and Cryosat-2 using OWL-Net data

Property		Value
Dynamic Model		EGM96 $40 \times 40$
		$3^{\text{rd}}$ body gravity
		(Sun, Moon and 9 planets, DE405)
		Solar Radiation Pressure
	Air drag (Jacchia-Roberts)	
<i>A priori</i> states		Result of Gauss method
Estimation	Convergence Criteria	$10^{-3}$

usually eliminates part of the measurement of the threshold such as  $3\sigma$  (Long et al. 1989). After data editing, the RA and DEC residuals are 74 and 28 arcsec, respectively (Fig. 10). The estimated RA bias is  $-0.0569^\circ$  and the DEC bias is  $0.0590^\circ$ .

### 4.3 Orbit Quality Assessment

The results were compared with the two-line elements

(TLE) of the corresponding satellite to determine the accuracy of the estimation. The direct comparison of the Cartesian states, however, is improper because the estimated ephemeris has an accumulated error due to the epoch state and system errors. For this reason, the estimation result is compared with TLE in form of mean orbital elements, which do not change much due to orbital motion (Table 4). The estimation of the bias shows that the difference of the orbital elements with respect to TLE is smaller in both satellites. The differences of the semi-major axis (SMA), inclination, and right ascension of the ascending node (RAAN) are  $< 1\%$ . Because both orbits are almost circular, the arguments of the perigee and mean anomaly do not match well but their sums (argument of latitude) do. The eccentricity, however, is estimated to be several times the TLE, which might be due to the velocity error.

Furthermore, the result of the Cryosat-2 estimate was



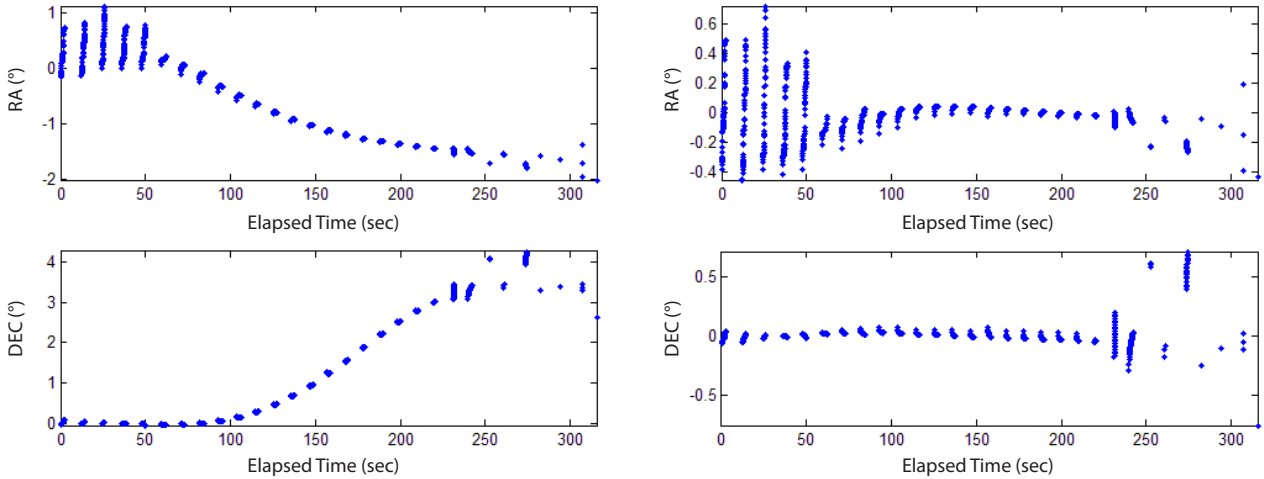


**Fig. 9.** *A priori* residual (left) and final residual after convergence (right) in the case of Cryosat-2. The residual reduced from several degrees to  $\sim 0.1^\circ$  and is exceptionally large in the beginning and end of the observation.

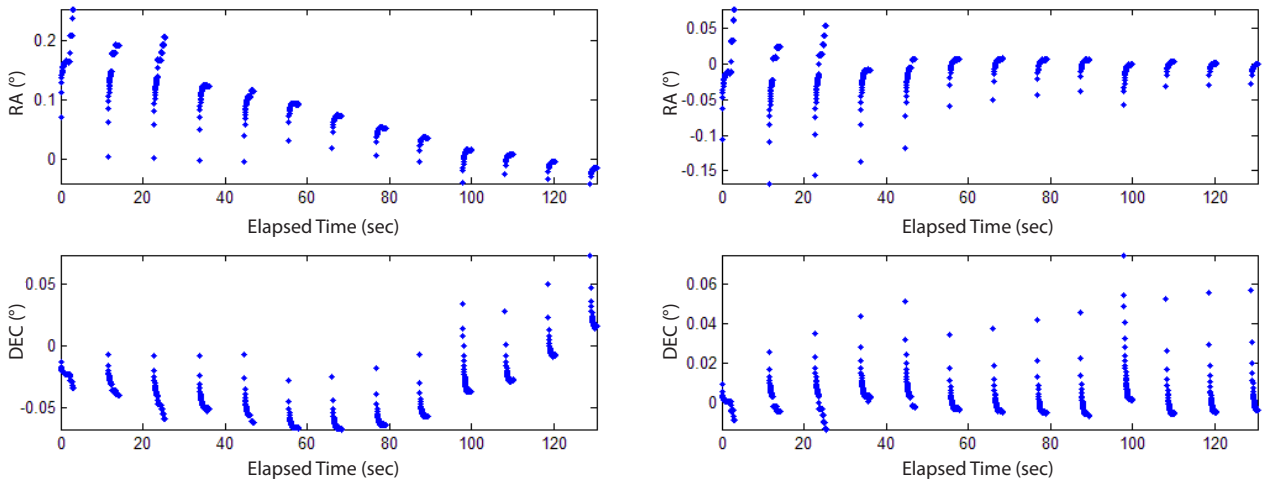


**Fig. 10.** The edited residual *a priori* (left) and after convergence (right) in the case of Cryosat-2. The RA and DEC residual change from  $\sim 0.1^\circ$  to 74 and 28 arc seconds, respectively.

**Table 4.** OD result using OWL-Net data of KOMPSAT-1 and Cryosat-2

	KOMPSAT-1			Cryosat-2		
	TLE	w/o bias (%)	With bias (%)	TLE	w/o bias (%)	With bias (%)
SMA (km)	7,046.0072	7,025.3128 (-0.2937)	7,035.2137 (-0.1532)	7,096.8249	7,105.6220 (0.1240)	7,100.5171 (0.0520)
ECC	0.0006215	0.001639 (163.7827)	0.002030 (226.6122)	0.0009738	0.002441 (150.7478)	0.001998 (100)
INC ( $^\circ$ )	97.7585	97.8411 (0.0845)	97.7406 (0.0183)	92.0277	92.0404 (0.0138)	92.0124 (-0.0166)
RAAN ( $^\circ$ )	121.5607	121.3772 (-0.1510)	121.2336 (-0.2691)	20.0517	19.8592 (0.9601)	19.8877 (-0.8180)
AOP ( $^\circ$ )	95.0345	184.5769 (94.2210)	143.1552 (-50.6350)	37.6167	111.7653 (197.1159)	95.4224 (153.6700)
MA ( $^\circ$ )	306.4787	217.1521 (-29.1461)	258.5401 (-15.6417)	99.6421	23.3999 (-76.5160)	39.7498 (-60.1075)

The OD is conducted with and without bias estimation and both results are compared with TLE in form of mean orbital elements. The difference ratio of the orbital elements with respect to TLE is smaller when the bias is estimated in both satellites.

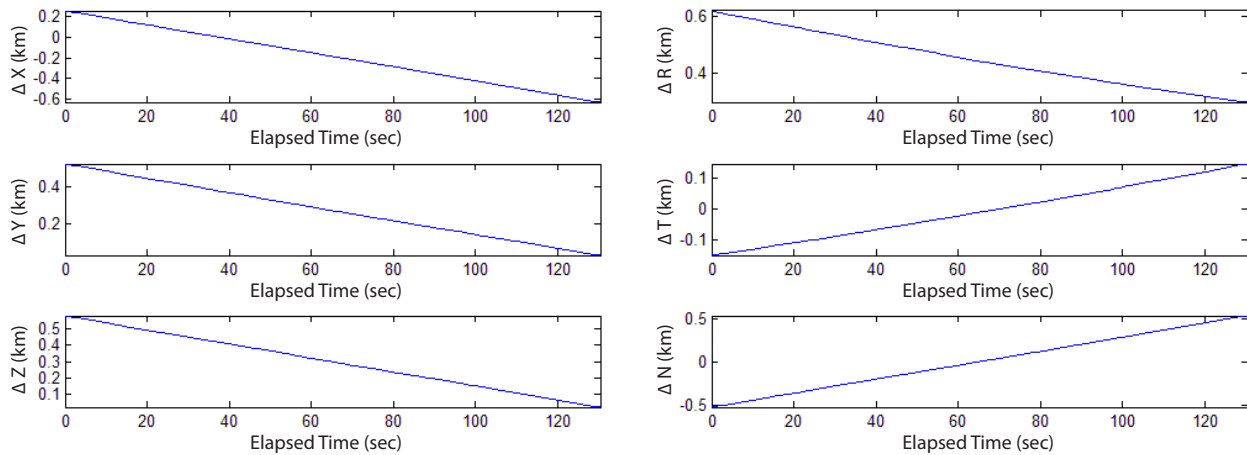


**Fig. 11.** Position difference of the estimation with respect to SLR ephemeris of Cryosat-2 in ITRF (left) and RTN coordinates (right). Each reference point is interpolated by the tenth order polynomial. The position difference mostly corresponds to the radial component.

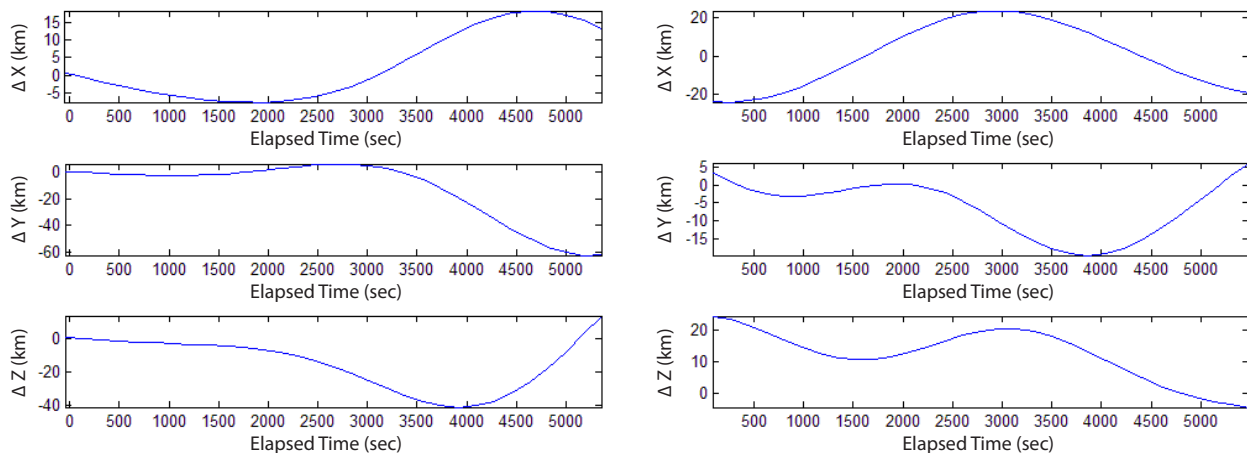


**Fig. 12.** Position difference of the estimated orbit (left) and TLE (right) with respect to SLR ephemeris of Cryosat-2 in the ITRF. Both trajectories are predicted for 90 min, that is, an orbital period. The position error is minimal at the epoch time and increases over time.

compared with the reference trajectory, which was published in consolidated prediction format (CPF) based on the international laser ranging system (ILRS) (Pearlman et al. 2002). The predicted trajectory is generated by prediction centers and regularly checked by several analytic centers, such as the Natural Environment Research Council (NERC); the accuracy is approximately several hundreds of meters (NERC Space Geodesy Facility 2017). It presents the three-dimensional position in the true-body-fixed of date system of the international terrestrial reference frame (ITRF). In this study, CPF data provided by ESA were used to analyze, where the epoch time of the trajectory is at 0:00 am on May 25, 2015, which is consistent with the observation date; the time interval of the position is 3 min. Fig. 11 shows the position difference in ITRF and RTN coordinates; each reference point is interpolated by the tenth order polynomial. The position difference at the epoch is ~0.8 km and most of the difference

corresponds to the radial component and to the result of the simulation in Subsection 3.1. The result is similar to the results of previous studies, which reported that the RMS difference between TLE and the estimated orbit is < 10 km in case of Cryosat-2 (Park et al. 2015).

Considering the field of view of the OWL-Net, which is 1.75° (Park et al. 2012), the position error of the LEO satellites should be lower than 20 km at the next arc for tracking. Fig. 12 shows the position difference of the estimated orbit and TLE with respect to the reference trajectory in ITRF. Both are propagated for 90 min, a period of the LEO satellite; the maximum position difference of the estimation is ~70 km, while the TLE difference is ~30 km. This might be due to the velocity difference, which is also related to the eccentricity error. The estimation accuracy can be improved by resolving unknown error sources of the OWL-Net (Jo et al. 2015).

Based on the error analysis that shows that the precision

of the measurement data is the same as that of the residual, the precision of the OWL-Net observation data is tens of arcsec. Based on the bias estimation, the accuracy of the observation data is also determined to be of sub-degree level.

## 5. SUMMARY AND CONCLUSIONS

Optical observation is suitable for the surveillance of space objects. The OWL-Net is a Korean optical surveillance system that tracks and monitors domestic satellites. In this study, the orbital states of two LEO satellites were determined using OWL-Net data and a batch least squares filter, which was developed and statistically verified. In addition, the precision and accuracy of OWL-Net data were analyzed based on the results of software simulations for error analysis.

The batch least squares filter processes all data to determine the epoch states; it is more robust to temporal measurement errors. The objective function is defined as the sum of the weighted residual and difference of the *a priori* states. The system model is composed of dynamic and measurement models. In this study, GMAT was utilized as the dynamic model and geometric RA/DEC was used as the measurement model. The system model was linearized to estimate the most probable epoch states; it turns into the states transition matrix and sensitivity matrix, where each matrix is numerically evaluated and analytically derived.

For statistical verification, Monte Carlo simulation was performed under two different conditions (unbiased measurement data without bias estimation; biased measurement data with bias estimation) and the results were compared with the covariance matrix. The results correspond to the multivariate analysis of the covariance in both cases, where 97 % of the estimation results plot inside the  $3\sigma$  covariance ellipsoid.

Potential error sources of OWL-Net, noise, bias, and clock errors were analyzed using software simulations. The estimation accuracy depends linearly on the noise level and the declination bias has a significant influence on the estimation in a polar orbit. The estimation converges only with a DEC bias larger than approximately  $-2^\circ$  and the estimation error increases to  $> 100$  km when the DEC bias is larger than  $2^\circ$ . This is due to the orbital characteristics, although it is not the general feature. Two types of clock errors were analyzed, time synchronization offset and time-tagging error. The position error is  $\sim 7.6$  km at a time-synchronization offset of 1 sec, which corresponds to an orbital velocity of  $\sim 8$  km/s of LEO. The time-tagging error, however, increases the position error up to 90 km because it

leads to irregular observation data.

The OWL-Net measurement data of KOMPSAT-1 and Cryosat-2 were provided by KASI and applied to the batch least squares algorithm. The Cartesian states were estimated by default and the measurement bias was optionally estimated. The estimated orbital states of both satellites are similar to those of TLE; however, the eccentricity error is significantly large. In case of Cryosat-2, the estimated trajectory was compared to the CPF trajectory in ITRF. Its difference is 0.8 km at the epoch time, which is similar to that of TLE and is in agreement with previous results (Park et al. 2015). However, the difference is  $\sim 70$  km after 90 min, while the corresponding value of TLE is  $\sim 30$  km. The precision of the OWL-Net data is tens of arcsec and the accuracy is of sub-degree level.

This study has nobility to demonstrate the operating capability of independent optical surveillance system of space objects. Unlike previous studies, which employed commercial software to examine OWL-Net measurement data, this study utilizes newly developed OD software. The results are similar to those of TLE. Because the software was statistically verified and examined under various conditions, the results are reliable and indicate the possibilities of independent space surveillance operations. The position error, however, increased when orbit propagation was performed, which might be due to the velocity error and can be improved through the use of parameter tuning and nonlinear estimation techniques. Furthermore, the precision and accuracy of OWL-Net measurement data was determined by interpreting the OD results. The performance of the OWL-Net can be improved by stabilizing the system to resolve unknown error sources; other reliable optical measurements can be used to check the performance of the OD software and analyze OWL-Net measurement data in the future.

## ACKNOWLEDGMENTS

This research was supported by Korea Astronomy and Space Science Institute (KASI) for orbit analysis using optical measurement data from OWL-Net.

## REFERENCES

- Crassidis JL, Junkins JL, Optimal estimation of dynamic systems, second edition (CRC press, New York, 2011).
- Henize KG, Stanley JF, O'Neill CA, Nowakowski BS, Detection of orbital debris with GEODSS telescopes, In Proc. SPIE 1951, 76-84 (1993). <https://dx.doi.org/10.1117/12.156562>
- Hughes SP, Qureshi RH, Cooley DS, Parker JJ, Grubb TG,

- Verification and validation of the general mission analysis tool (GMAT), in 2014 AIAA/AAS Astrodynamics Specialist Conference, San Diego, CA, 4-7 Aug 2014.
- Jo JH, Choi J, Park M, Son JY, Bae Y, et al., Early CAL/VAL process for an optical tracking system by Korea, Proceedings of the 16th AMOS Conference, Maui, Hawaii, 15-18 Sep 2015.
- Kim HO, Kim HS, Lim HS, Choi HJ, Space-based earth observation activities in south Korea [Space Agencies], IEEE Geosci. Remote Sens. Mag. 3, 34-39 (2015). <https://doi.org/10.1109/MGRS.2014.2382652>
- Kurtz NT, Galin N, Studinger M, An improved CryoSat-2 sea ice freeboard retrieval algorithm through the use of waveform fitting, Cryosphere 8, 1217-1237 (2014). <https://dx.doi.org/10.5194/tcd-8-721-2014>
- Long AC, Cappellari Jr. JO, Velez CE, Fuchs AJ, Goddard trajectory determination system (GTDS) mathematical theory (revision 1), National Aeronautics and Space Administration/Goddard Space Flight Center, FDD/552-89/001, CSC/TR-89/6001 (1989).
- Molotov I, Agapov V, Titenko V, Khutorovsky Z, Burtsev Y, et al., International scientific optical network for space debris research, Adv. Space Res. 41, 1022-1028 (2008). <https://dx.doi.org/10.1016/j.asr.2007.04.048>
- NERC Space Geodesy Facility, Satellite CPF Prediction Residuals [Internet], cited 2017 Feb 15, available from: <http://sgf.rgo.ac.uk>
- Park J, Choi Y, Jo J, Moon H, Im H, et al., A Korean space situational awareness program: OWL Network, Proceedings of the Advanced Maui Optical and Space Surveillance Technologies Conference, Maui, Hawaii, 11-14 Sep 2012.
- Park M, Jo JH, Cho S, Choi J, Kim CH, et al., Minimum number of observation points for LEO satellite orbit estimation by OWL Network, J. Astron. Space Sci. 32, 357-366 (2015). <https://dx.doi.org/10.5140/JASS.2015.32.4.357>
- Park SY, Keum KH, Lee SW, Jin H, Park YS, et al., Development of a data reduction algorithm for optical wide field patrol, J. Astron. Space Sci. 30, 193-206 (2013). <https://dx.doi.org/10.5140/JASS.2013.30.3.193>
- Pearlman MR, Degnan JJ, Bosworth JM, The international laser ranging service, Adv. Space Res. 30, 135-143 (2002). [https://dx.doi.org/10.1016/S0273-1177\(02\)00277-6](https://dx.doi.org/10.1016/S0273-1177(02)00277-6)
- Sabol C, Alfriend KT, Wiese D, Angles-only orbit updates for low-earth-orbit satellites, J. guid. Control. Dyn. 30, 314-321 (2007). <https://dx.doi.org/10.2514/1.25008>
- Schutz B, Tapley B, Born GH, Statistical orbit determination, first edition (Academic Press, San Diego, 2004).
- Son JY, Jo JH, Choi J, Kim BY, Yoon JN, et al., Optical orbit determination of a Geosynchronous Earth Orbit satellite effected by baseline distances between various ground-based tracking stations II: COMS case with analysis of actual observation data, J. Astron. Space Sci. 32, 229-235 (2015). <https://dx.doi.org/10.5140/JASS.2015.32.3.229>
- Stokes GH, Evans JB, Viggh HE, Shelly FC, Pearce EC, Lincoln near-Earth asteroid program (LINEAR), Icarus 148, 21-28 (2000). <https://dx.doi.org/10.1006/icar.2000.6493>
- Tombasco J, Orbit estimation of geosynchronous objects via ground-based and space-based optical tracking, PhD Dissertation, University of Colorado (2011).
- Vallado DA, Agapov V, Orbit determination results from optical measurements, in AIAA/AAS Astrodynamics Specialist Conference, Toronto, Ontario, 2-5 Aug 2010.